THE JOURNAL OF PHYSICAL CHEMISTRY Letters

Letter

Cite This: J. Phys. Chem. Lett. 2020, 11, 445−450

pubs.acs.org/JPCL

Monitoring Charge Carrier Diffusion across a Perovskite Film with Transient Absorption Spectroscopy

Hannu P. Pasanen,*[,†] Paola Vivo,[†] Laura Canil,[‡] Hannes Hempel,[‡] Thomas Unold,[‡] Antonio Abate,[‡,¶] and Nikolai V. Tkachenko*[,†]

[†]Chemistry and Advanced Materials Group, Faculty of Engineering and Natural Sciences, Tampere University, Korkeakoulunkatu 8, FI-33720 Tampere, Finland

[‡]Helmholtz-Zentrum Berlin für Materialien und Energie, Kekuléstraße 5, 12489 Berlin, Germany

[¶]Materials and Production Engineering, University of Naples Federico II, Piazzale Tecchio 80, Fuorigrotta, 80125 Naples, Italy

Supporting Information

ABSTRACT: We have developed a new noninvasive optical method for monitoring charge carrier diffusion and mobility in semiconductor thin films in the direction perpendicular to the surface which is most relevant for devices. The method is based on standard transient absorption measurements carried out in reflectance and transmittance modes at wavelengths below the band gap where the transient response is mainly determined by the change in refractive index, which in turn depends on the distribution of photogenerated carriers across the film. This distribution is initially inhomogeneous because of absorption at the excitation wavelength and becomes uniform over time via diffusion. By modeling these phenomena we can determine the diffusion constant and respective mobility. Applying the method to a 500 nm thick triple cation FAMACs perovskite film revealed that homogeneous carrier distribution is established in few hundred picoseconds, which is consistent with mobility of 66 $cm^2 (V s)^{-1}$.

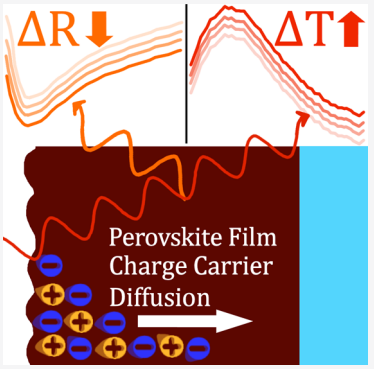

Charge carrier mobility is one of the most important parameters for materials in applications such as solar cells, but it is notoriously difficult to measure. New contact-free measurement techniques have been sought in order to avoid the problems faced by contact methods[1−4] (the need to apply voltage across the sample, diffusion of ions due to the voltage, and electrode−film interface complications), but so far the optical methods[5−7] have mainly been able to measure intragrain mobility with some exceptions for measuring mobility parallel to the film surface.[8,9] This is problematic because mobility perpendicular to the film surface is often more relevant for practical applications: The intragrain mobility and mobility over multiple grain boundaries can differ by orders of magnitude,[10,11] while the perpendicular mobility is somewhere between these two extremes. Our new contact-free method presented in this Letter allows us to determine this mobility across thin films.

It has been shown that the photoinduced change in refractive index influences visible range transient absorption (TA) measurements,[12,13] and transient reflectance (TR) has been utilized in determination of charge mobility; however, these techniques were limited to measuring parallel mobility[11] or acquiring the signal only from the sample surface,[14] making it prone to various surface effects. In our previous paper we examined the transient absorption and reflectance signals coming from metal halide perovskite (FAMACs-perovskite) thin film on glass and found that in the near-infrared (NIR) photoinduced transmittance change is dominated by the refractive index change.[15] At these sub-band gap wavelengths the FAMACs-perovskite has low absorption, and thus the reflectance depends on thin-film interference. Essentially the reflectance is influenced by the entire film instead of being determined only by the air−film interface. Thus, the reflectance is affected by spatial differences in the refractive index, which can be generated by an uneven distribution of charge carriers after excitation. The carrier distribution becomes uniform over time via diffusion, appearing as a transient signal in transient reflectance and transmittance spectroscopy even when the total number of carriers remains the same. In this study we model these phenomena and utilize them to determine the diffusion and mobility of charge carriers in a perovskite film. The diffusion constant acquired in this contact-free manner represents the diffusion of charge carriers perpendicularly through the film. It also avoids the problem of ion diffusion thanks to the fast time scale and lack of strong electric field. Our method is easy to adapt as it requires only standard transient absorption equipment with minor modifications to measure the reflected probe beam in addition to the transmitted probe, and the analysis can be extended to include various other phenomena such as interfacial effects.

In this study we used perovskite films prepared following the procedure described by Saliba et al. for high-efficiency

Received: November 20, 2019
Accepted: December 20, 2019
Published: December 20, 2019

DOI: 10.1021/acs.jpclett.9b03427
J. Phys. Chem. Lett. 2020, 11, 445−450

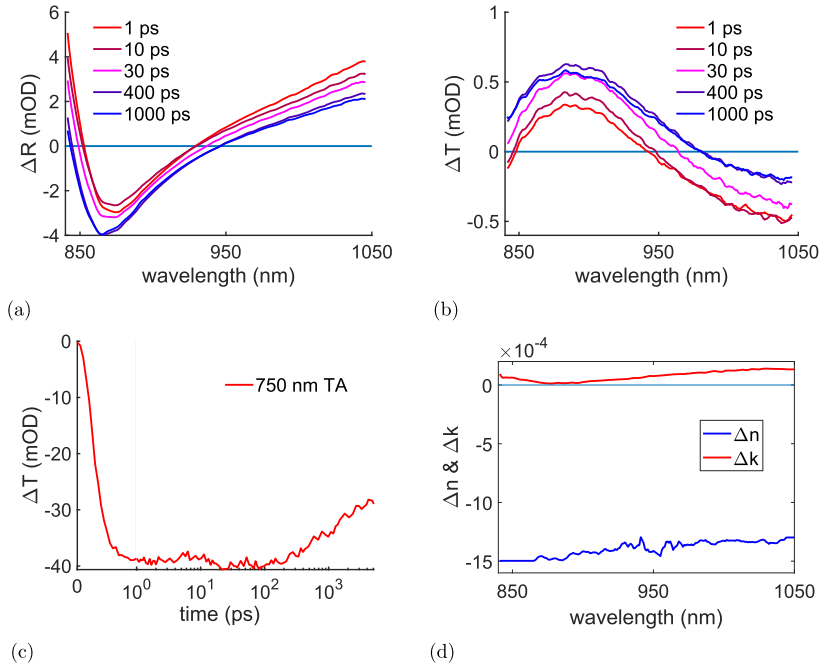

Figure 1. Time-resolved transient reflectance (a) and transmittance (b) spectra of perovskite layer in NIR with pump wavelength of 530 nm. (c) TA response at the band gap (750 nm) showing no significant recombination during initial 400 ps. The plot is linear up to 1 ps as denoted by the green line. (d) Estimated change of refractive index and extinction coefficient when charge distribution is uniform (1 ns delay). Excitation density was approximately 3 $\mu J/cm^2$, and pump repetition rate was 500 Hz.

perovskite solar cells.[16] The composition is FAMACs-perovskite, i.e., the so-called "triple cation perovskite" (formamidinium (FA), methylammonum (MA), and cesium), which is well-known for giving solar cells with good stability and efficiencies exceeding 20%.[16−18] FAMACs-perovskite is a widely investigated material[19−21] derived from the well-known methylammonium lead iodide ($MAPbI_3$) and $FA_xCs_{1-x}Pb(Br_yI_{1-y})_3$. Their charge carrier mobilities have also been reported, with values typically ranging from 20 to 40 $cm^2\ (V\ s)^{-1}$.[10,20,22] FAMACs has similar optoelectronic properties as $MAPbI_3$, but it displays enhanced stability; thus, it can be a considered a more reliable reference material to test the technique. According to a visible range TA measurement (Figure 1c, full spectra in Figure S6), our samples had long lifetime in nanosecond scale without recombination or other changes in signal during initial 400 ps, and they consisted of a 500 nm perovskite layer on top of glass without any additional layers to avoid interfacial effects.

Transfer matrix is a method for simulating thin-film reflectance and transmittance,[23] and it can also be used to simulate transient absorption and reflectance responses simply by calculating the relative difference in reflectance after changing the complex refractive index, as we did previously.[15] The change in complex refractive index is $\Delta\tilde{n} = \Delta n + i\Delta k$, where n is the real part of the refractive index and k is the extinction coefficient related to absorption coefficient via $\alpha = 2\pi k/\lambda$, where λ is the wavelength.

The transfer matrix method can also be applied to a multilayered system and be used to simulate the effect of nonuniform refractive index distribution. We split the perovskite film into multiple layers, each with change in complex refractive index proportional to the charge carrier density in that layer at the given time. The spectral change in refractive index was acquired as in our previous paper[15] by taking the spectra at long delay time (1 ns), assuming a uniform distribution of charge carriers at that delay time and calculating the change in refractive index. To estimate the steady-state refractive index we used the refractive index of $MAPbI_3$ perovskite reported by Phillips et al.[24] with minor modifications to match the band gap, the validity of which was verified in our previous paper[15] by analyzing steady-state spectra.

Our model of the perovskite film included surface roughness on top of the bulk perovskite. Roughness was necessary to adjust the simulated transient reflectance signal at early delay times, which is discussed later in the results. The roughness was modeled as a nanocone top layer which has an effect of smoothing the change of refractive index at the interface, and the total volume of perovskite with and without roughness layer was kept approximately the same (see the Supporting Information for details). The bulk perovskite was split into 200 layers, and the nanocone was split into 90 layers for the transfer matrix.

Diffusion and charge carrier density distribution was simulated using Matlab pdepe-function[25] in one dimension. The diffusion equation is

$$\frac{\partial u}{\partial t} = D\frac{\partial^2 u}{\partial x^2} - R \tag{1}$$

where u is the carrier density distribution over the sample, D the diffusion constant, and R the recombination of carriers; t and x are time and location, respectively. Boundary conditions were that there was no flux over the boundaries; in other words, the derivative of u across boundary was zero, and surface recombination is neglected. The initial carrier density distribution was calculated as Lambert−Beer type. Because the main diffusion is found to occur on time scales much faster than the carrier recombination even under high injection conditions, we have approximated $R = u/\tau$ with a constant

DOI: 10.1021/acs.jpclett.9b03427
J. Phys. Chem. Lett. 2020, 11, 445−450

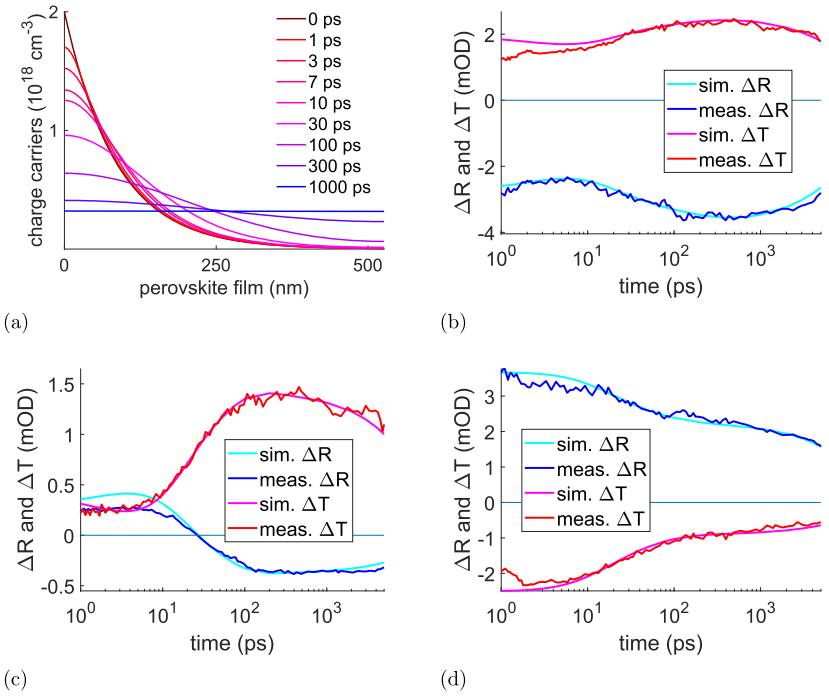

Figure 2. Simulated (a) charge carrier density distributions and (b–d) resulting transient reflectance and transmittance signals at wavelengths 880, 936, and 1040 nm, respectively. Surface roughness was included in this simulation; the diffusion constant was 1.64 cm^2 s^{-1}, and the lifetime was 14.7 ns. ΔT was multiplied by 4 for clarity.

lifetime (τ), which is significantly greater (>10 ns) than the time window considered in the experiment.

Diffusion constant D fitting was done by minimizing the root-mean-square deviation between the simulated time-resolved response and experimental data. Diffusion constant was the only fitting parameter, and the fit was done separately at each wavelength. The corresponding mobility μ was calculated as

$$\mu = \frac{eD}{k_B T} \tag{2}$$

where e is the elementary charge, k_B Boltzmann's constant, and T the temperature.

The steps for the entire method (after determining the correct bulk and roughness thicknesses) are as follows:

(1) Determine photoinduced change in complex refractive index at a long delay time (1 ns) where charge carrier distribution is uniform.
(2) Model charge carrier distribution at each delay time. These distributions depend on charge carrier mobility, film thickness, and charge carrier lifetime.
(3) Model transient reflectance and transmittance responses with charge carrier distributions from step 2 and photoinduced change in refractive index acquired in step 1.
(4) Fit the simulated transient signal to the measured data by adjusting the diffusion constant.

More detailed instructions and Matlab-codes for each step are found in the Supporting Information.

Figure 1a,b shows the evolution of the transient transmittance and reflectance responses in NIR. The pump wavelength was 530 nm at which absorbance of the sample is 2.7 after accounting for reflectance. The hot carriers cool during the first picosecond (Figure S4).[26] From 1 to 6 ps both the transient reflectance and transmittance shift up at 880 nm, although the changes should be opposite (one shifts up and the other down) if only refractive index was changing.[15] Then from 6 ps to few hundred picoseconds the reflectance signal behaves in an uncommon way: the entire spectral response moves down without changing shape. The transmittance signal behaves in an exactly opposite manner, as expected if there is no change in absorption and only refractive index is changing. From 400 ps onward the main effect on the signal is the slow recombination of charge carriers.

We estimated the change in refractive index from the signal around 1 ns (Figure 1a,b), which proved to be essentially flat (Figure 1d). We then simulated the diffusion of charge carriers (Figure 2a) and the corresponding transient reflectance and absorption signals (Figure 2b–d). Interestingly, the initial decay of the reflectance signal at 880 nm corresponds to charge carrier distribution becoming more flat near the surface of the perovskite film (1–6 ps), and then the entire reflectance signal moves down as the distribution becomes uniform (6–400 ps).

According to Figure 2b the transmittance signal should also decrease when the reflectance signal decreases during early delay times (1–6 ps). However, at 1 ps the transmittance signal is already too small, and instead it increases while reflectance signal decreases. This implies that there is a process with a short lifetime that results in a negative change in absorption at 880 nm, possibly caused by defects in the perovskite. Apart from these small deviations the simulation reproduces the experimental signals with reasonable accuracy.

Figure 3 shows the effect of adding roughness to the model: Without roughness the simulated reflectance at 1 ps delay at 880 nm is too weak, although it otherwise reproduces the transient features correctly. The flat surface model overestimates the effect of charge carrier distribution on the signal, meaning that the more roughness there is, the weaker the transient features from diffusion become. However, it should

DOI: 10.1021/acs.jpclett.9b03427
J. Phys. Chem. Lett. 2020, 11, 445–450

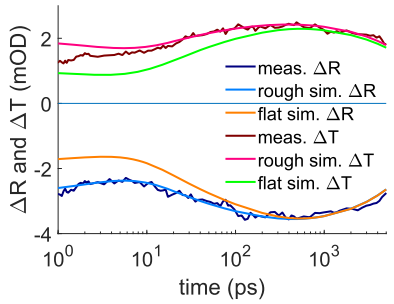

Figure 3. Effect of surface roughness on transient reflectance and transmittance simulations at 880 nm. Transmittance signal was multiplied by 4 for clarity.

be noted that the exact effect of roughness depends on the wavelength (Figure S4). The thickness of roughness in the model was adjusted until the simulated reflectance signal at 1 ps matched the measured signal. The accuracy of the method is thereby limited by knowledge of the film structure and carrier recombination and the accuracy of the instrument itself.

The diffusion constant was fitted separately at each wavelength, and the results of the fit are shown in Figure 4.

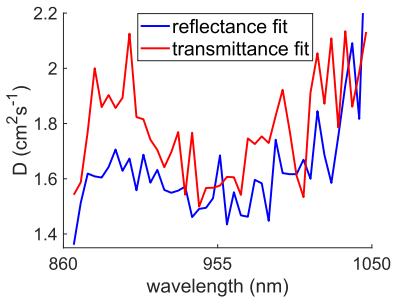

Figure 4. Diffusion constant acquired by fitting simulated transient signal to measured signal at each wavelength.

Average diffusion constant was 1.64 ± 0.15 $cm^2\,s^{-1}$ for the reflectance signal fit and 1.78 ± 0.14 $cm^2\,s^{-1}$ for the transmittance. Assuming common ambipolar diffusion of electrons and holes during the measurement and equal mobilities of both carrier kinds, this leads to average charge carrier mobility of 66 ± 8 $cm^2\,(V\,s)^{-1}$. This value is higher than typically reported mobility measurements done on $MAPbI_3$ and other similar perovskite films,[10] but it is within reasonable limits. If ambipolar diffusion does not apply, meaning that one carrier type moves much faster than the other, then the method gives a weighted average based on which carrier type is more responsible for the change in refractive index. The two carrier types can also be modeled separately by each having their own diffusion constant and change in complex refractive index and then combining their effects for transfer matrix simulation.

To further evaluate our results we performed time-resolved terahertz spectroscopy (TRTS) on a similar sample (details are provided in the Supporting Information). It measured a sum of the electron mobility and of the hole mobility of 65 ± 10 $cm^2\,(V\,s)^{-1}$. The corresponding average mobility, 32.5 $cm^2\,(V\,s)^{-1}$, is half of the mobility acquired with our new transient reflectance method. Because TRTS primarily measures short-distance mobility within single grains of the polycrystalline film and transient reflectance measures diffusion through the film, we expected the TRTS to provide higher mobility compared to transient reflectance. However, two times difference is not uncommon among different mobility measurement techniques, and our result from transient reflectance matches many reported values for single-crystal measurements,[10] although the variance in single-crystal results is high. It could also be that the diffusion is not ambipolar, causing the transient reflectance method to mainly measure the faster charge carrier that has higher impact on the refractive index, explaining some of the difference in results. In total, we can conclude that charge carriers in FAMACs perovskite films travel within single grains from top to bottom and crystal boundaries do not significantly limit mobility.

In conclusion, we have developed a new contact-free method to monitor charge carrier diffusion in semiconductor thin films using transient reflectance and transmittance spectroscopy with a standard pump−probe instrument, which can potentially be further adapted to study various diffusion-impacted phenomena such as interfacial charge transfer rates. Unlike most methods for measuring carrier diffusion or mobility, our method allows their determination perpendicular to the film surface, which is highly relevant for practical applications. This was achieved by modeling the effect of nonuniform charge carrier distribution on transient reflectance and transmittance signals and analyzing how diffusion and other effects such as film roughness influence them. The method was applied to study the charge carrier mobility in a triple-cation FAMACs perovskite film, yielding a carrier mobility value of 66 ± 8 $cm^2\,(V\,s)^{-1}$. The result was compared with TRTS which provides intragrain mobility, allowing us to conclude that the charge carriers in FAMACs perovskite films are not significantly hindered by crystal boundaries and can travel from top to bottom within a single crystal. The requirements of our method are that the film is of sufficient quality (uniform, low roughness, low scattering, etc.), the carrier lifetime is longer than the diffusion effect, and that the film has sufficient absorption at the pump wavelength to generate the required initial charge carrier distribution.

EXPERIMENTAL METHODS

FAMACs-perovskite synthesis and sample fabrication are described in detail in the Supporting Information.

Ultrafast transient reflectance and transmittance responses of the samples were measured in ambient conditions using a pump−probe system described previously.[27,28] Equipment details are provided in the Supporting Information. Briefly, the samples were excited by laser pulses at 530 nm with an excitation density of approximately 3 $\mu J/cm^2$. The optimal pump flux was determined in our previous paper with similar samples.[15] The responses were measured using an ExciPro transient absorption spectrometer. The pulse repetition rate of the laser system was 1 kHz, and the spectra were typically acquired by averaging over 5 s. The time resolution of the instrument was 100 fs. The sample was tilted 10° to allow both transmittance and reflectance mode measurements. In the reflectance mode the probe light reflected from the sample was directed to the detection system by a mirror placed in front of the sample.

The time-resolved terahertz spectroscopy setup was described in an article by Hempel et al.,[29] and the technique is described in more detail in the Supporting Information. In this study the pump pulse had wavelength of 402 nm and the photon flux was 4 × 10^{12} photons/cm^2 per pulse.

DOI: 10.1021/acs.jpclett.9b03427
J. Phys. Chem. Lett. 2020, 11, 445−450

■ ASSOCIATED CONTENT

Supporting Information

The Supporting Information is available free of charge at https://pubs.acs.org/doi/10.1021/acs.jpclett.9b03427.

Additional details on how the modeling was done (roughness layer, extra details on each modeling step, recombination-free transient simulation, and visible range transient reflectance simulations), visible range TA, sample absorbance spectra, experimental details (time-resolved terahertz spectroscopy, transient absorption equipment, and sample fabrication) (PDF)

Matlab codes: matlab codes for modeling effect of diffusion on transient signals and fitting diffusion constant (ZIP)

■ AUTHOR INFORMATION

Corresponding Authors

*E-mail: hannu.pasanen@tuni.fi.

*E-mail: nikolai.tkachenko@tuni.fi.

ORCID

Hannu P. Pasanen: 0000-0002-7237-2677

Paola Vivo: 0000-0003-2872-6922

Thomas Unold: 0000-0002-5750-0693

Antonio Abate: 0000-0002-3012-3541

Nikolai V. Tkachenko: 0000-0002-8504-2335

Notes

The authors declare no competing financial interest.

■ ACKNOWLEDGMENTS

The work is part of the Academy of Finland Flagship Programme, Photonics Research and Innovation (PREIN), decision 320165. P.V., L.C., and A.A. thank Business Finland and Forschungszentrum Jülich GmbH (SolarWAVE project) for financial support. P.V. also thanks Jane & Aatos Erkko foundation (project ASPIRE). H.P.P. thanks the doctoral program of Tampere University for financial support.

■ REFERENCES

(1) Bercegol, A.; Ramos, F. J.; Rebai, A.; Guillemot, T. J.-B.; Puel; Guillemoles, J.-F.; Ory, D.; Rousset, J.; Lombez, L. Spatial Inhomogeneity Analysis of Cesium-Rich Wrinkles in Triple-Cation Perovskite. *J. Phys. Chem. C* **2018**, *122*, 23345−23351.

(2) Shi, D.; Adinolfi, V.; Comin, R.; Yuan, M.; Alarousu, E.; Buin, A.; Chen, Y.; Hoogland, S.; Rothenberger, A.; Katsiev, K.; et al. Low Trap-State Density and Long Carrier Diffusion in Organolead Trihalide Perovskite Single Crystals. *Science* **2015**, *347*, 519−522.

(3) Stoumpos, C. C.; Malliakas, C. D.; Kanatzidis, M. G. Semiconducting Tin and Lead Iodide Perovskites with Organic Cations: Phase Transitions, High Mobilities, and Near-Infrared Photoluminescent Properties. *Inorg. Chem.* **2013**, *52*, 9019−9038.

(4) Dong, Q.; Fang, Y.; Shao, Y.; Mulligan, P.; Qiu, J.; Cao, L.; Huang, J. Electron-Hole Diffusion Lengths > 175 μm in Solution-Grown $CH_3NH_3PbI_3$ Single Crystals. *Science* **2015**, *347*, 967−970.

(5) Milot, R. L.; Eperon, G. E.; Snaith, H. J.; Johnston, M. B.; Herz, L. M. Temperature-Dependent Charge-Carrier Dynamics in $CH_3NH_3PbI_3$ Perovskite Thin Films. *Adv. Funct. Mater.* **2015**, *25*, 6218−6227.

(6) Rehman, W.; Milot, R. L.; Eperon, G. E.; Wehrenfennig, C.; Boland, J. L.; Snaith, H. J.; Johnston, M. B.; Herz, L. M. Charge-Carrier Dynamics and Mobilities in Formamidinium Lead Mixed-Halide Perovskites. *Adv. Mater.* **2015**, *27*, 7938−7944.

(7) Hutter, E. M.; Eperon, G. E.; Stranks, S. D.; Savenije, T. J. Charge Carriers in Planar and Meso-Structured Organic-Inorganic Perovskites: Mobilities, Lifetimes, and Concentration of Trap States. *J. Phys. Chem. Lett.* **2015**, *6*, 3082−3090.

(8) Guo, Z.; Manser, J. S.; Wan, Y.; Kamat, P. V.; Huang, L. Spatial and Temporal Imaging of Long-Range Charge Transport in Perovskite Thin Films by Ultrafast Microscopy. *Nat. Commun.* **2015**, *6*, 7471.

(9) Biewald, A.; Giesbrecht, N.; Bein, T.; Docampo, P.; Hartschuh, A.; Ciesielski, R. Temperature-Dependent Ambipolar Charge Carrier Mobility in Large-Crystal Hybrid Halide Perovskite Thin Films. *ACS Appl. Mater. Interfaces* **2019**, *11*, 20838−20844.

(10) Herz, L. Charge-Carrier Mobilities in Metal Halide Perovskites: Fundamental Mechanisms and Limits. *ACS Energy Lett.* **2017**, *2*, 1539−1548.

(11) Lim, J.; Hörantner, M. T.; Sakai, N.; Ball, J. M.; Mahesh, S.; Noel, N. K.; Lin, Y.-H.; Patel, J. B.; McMeekin, D. P.; Johnston, M. B.; et al. Elucidating the Long-Range Charge Carrier Mobility in Metal Halide Perovskite Thin Films. *Energy Environ. Sci.* **2019**, *12*, 169−176.

(12) Price, M. B.; Butkus, J.; Jellicoe, T. C.; Sadhanala, A.; Briane, A.; Halpert, J. E.; Broch, K.; Hodgkiss, J. M.; Friend, R. H.; et al. Hot-Carrier Cooling and Photoinduced Refractive Index Changes in Organic−Inorganic Lead Halide Perovskites. *Nat. Commun.* **2015**, *6*, 8420.

(13) Yang, Y.; Yang, M.; Moore, D. T.; Yan, Y.; Miller, E. M.; Zhu, K.; Beard, M. C. Top and Bottom Surfaces Limit Carrier Lifetime in Lead Iodide Perovskite Films. *Nature Energy* **2017**, *2*, 16207.

(14) Yang, Y.; Yan, Y.; Yang, M.; Choi, S.; Zhu, K.; Luther, J.; Beard, M. Low Surface Recombination Velocity in Solution-Grown $CH_3NH_3PbBr_3$ Perovskite Single Crystal. *Nat. Commun.* **2015**, *6*, 7961.

(15) Pasanen, H. P.; Vivo, P.; Canil, L.; Abate, A.; Tkachenko, N. Refractive Index Change Dominates the Transient Absorption Response of Metal Halide Perovskite Thin Films in the near Infrared. *Phys. Chem. Chem. Phys.* **2019**, *21*, 14663−14670.

(16) Saliba, M.; Correa-Baena, J.-P.; Wolff, C. M.; Stolterfoht, M.; Phung, N.; Albrecht, S.; Neher, D.; Abate, A. How to Make over 20% Efficient Perovskite Solar Cells in Regular (n−i−p) and Inverted (p−i−n) Architectures. *Chem. Mater.* **2018**, *30*, 4193−4201.

(17) Saliba, M.; Matsui, T.; Seo, J.-Y.; Domanski, K.; Correa-Baena, J.-P.; Nazeeruddin, M. K.; Zakeeruddin, S. M.; Tress, W.; Abate, A.; Hagfeldtd, A.; et al. Cesium-Containing Triple Cation Perovskite Solar Cells: Improved Stability, Reproducibility and High Efficiency. *Energy Environ. Sci.* **2016**, *9*, 1989−1997.

(18) Christians, J. A.; Schulz, P.; Tinkham, J. S.; Schloemer, T. H.; Harvey, S. P.; de Villers, B. J. T.; Sellinger, A.; Berry, J. J.; Luther, J. M. Tailored Interfaces of Unencapsulated Perovskite Solar Cells for > 1,000 h Operational Stability. *Nature Energy* **2018**, *3*, 68−74.

(19) Tan, H.; Che, F.; Wei, M.; Zhao, Y.; Saidaminov, M. I.; Todorović, P.; Broberg, D.; Walters, G.; Tan, F.; et al. Dipolar Cations Confer Defect Tolerance in Wide-Bandgap Metal Halide Perovskites. *Nat. Commun.* **2018**, *9*, 3100.

(20) Hu, Y.; Hutter, E. M.; Rieder, P.; Grill, I.; Hanisch, J.; Aygüler, M. F.; Hufnagel, A. G.; Handloser, M.; Bein, T.; Hartschuh, A.; et al. Understanding the Role of Cesium and Rubidium Additives in Perovskite Solar Cells: Trap States, Charge Transport, and Recombination. *Adv. Energy Mater.* **2018**, *8*, 1703057.

(21) Saidaminov, M. I.; Kim, J.; Jain, A.; Quintero-Bermudez, R.; Tan, H.; Long, G.; Tan, F.; Johnston, A.; Zhao, Y.; Voznyy, O.; et al. Suppression of Atomic Vacancies via Incorporation of Isovalent Small Ions to Increase the Stability of Halide Perovskite Solar Cells in Ambient Air. *Nature Energy* **2018**, *3*, 648−654.

(22) Rehman, W.; McMeekin, D. P.; Patel, J. B.; Milot, R. L.; Johnston, M. B.; Snaith, H. J.; Herz, L. M. Photovoltaic Mixed-Cation Lead Mixed-Halide Perovskites: Links Between Crystallinity, Photo-Stability and Electronic Properties. *Energy Environ. Sci.* **2017**, *10*, 361−369.

(23) Yariv, A.; Yeh, P. *Photonics: Optical Electronics in Modern Communications*, 6th ed.; Oxford University Press, 2007.

(24) Phillips, L. J.; Rashed, A. M.; Treharne, R. E.; Kay, J.; Yates, P.; Mitrovic, I. Z.; Weerakkody, A.; Hall, S.; Durose, K. Dispersion

DOI: 10.1021/acs.jpclett.9b03427
J. Phys. Chem. Lett. 2020, 11, 445−450

Relation Data for Methylammonium Lead Triiodide Perovskite Deposited on a (100) Silicon Wafer Using a Two-Step Vapour-Phase Reaction Process. *Data in Brief* **2015**, *5*, 926−928.
(25) Mathworks. Solve Initial-Boundary Value Problems for Parabolic-Elliptic PDEs in 1-D. https://www.mathworks.com/help/matlab/ref/pdepe.html (accessed September 9, 2019).
(26) Fu, J.; Xu, Q.; Han, G.; Wu, B.; Huan, C. H. A.; Leek, M. L.; Sum, T. C. Hot Carrier Cooling Mechanisms in Halide Perovskites. *Nat. Commun.* **2017**, *8*, 1300.
(27) Virkki, K.; Demir, S.; Lemmetyinen, H.; Tkachenko, N. V. Photoinduced Electron Transfer in CdSe/ZnS Quantum Dot-Fullerene Hybrids. *J. Phys. Chem. C* **2015**, *119*, 17561−17572.
(28) Stranius, K.; George, L.; Efimov, A.; Ruoko, T.-P.; Pohjola, J.; Tkachenko, N. V. Photophysical Study of a Self-Assembled Donor-Acceptor Two-Layer Film on TiO_2. *Langmuir* **2015**, *31*, 944−952.
(29) Hempel, H.; Unold, T.; Eichberger, R. Measurement of Charge Carrier Mobilities in Thin Films on Metal Substrates by Reflection Time Resolved Terahertz Spectroscopy. *Opt. Express* **2017**, *25*, 17227−17236.

DOI: 10.1021/acs.jpclett.9b03427
J. Phys. Chem. Lett. 2020, 11, 445−450